CLM - P 283

UKAEA RESEARCH GROUP

Preprint

AN EXPERIMENTAL AND TWO-DIMENSIONAL COMPUTATIONAL STUDY OF END LOSSES FROM A THETA PINCH

H A B BODIN
J McCARTAN
I K PASCO
W H SCHNEIDER

CULHAM LABORATORY
Abingdon Berkshire

1971

CLM-P 283

AN EXPERIMENTAL AND TWO-DIMENSIONAL COMPUTATIONAL STUDY OF END LOSSES FROM A THETA PINCH

by

H.A.B. Bodin, J. McCartan*, I.K. Pasco, W.H. Schneider+

A B S T R A C T

This paper describes a theoretical and experimental study of axial plasma flow and end losses in a theta pinch with a collisional 100 eV plasma with beta on axis of 0.7. The predictions of an M.H.D. code which is two-dimensional in radius and axial length were compared with data from a theta pinch with a coil 8 metres long, which gives stable times of some tens of microseconds and good axial resolution. The radial density distribution was measured at four axial positions and its spatial and temporal evolution during the loss process agreed with the computed results. Rarefaction waves were found numerically, and the propagation velocity on a given flux tube agreed with the analytic expression. The computed and measured line density also agreed, and fell sequentially at different axial positions. The results showed that particle flow on a given flux tube depends on the local values of beta and sound speed. Higher beta plasma on the axis is lost more slowly than the plasma as a whole.

* Killed in a climbing accident February 1970.

+ Present address: Institut für Plasmaphysik, Garching, West Germany.

U.K.A.E.A.,
Culham Laboratory,
Abingdon,
Berks.

September 1971

1. INTRODUCTION

Axial flow and end losses in theta pinches have been studied in collisional plasmas[1-3], in the high temperature collisionless regime[3-5] and in the reversed field[6-9] configuration. In addition, the effects of magnetic mirrors[3,10] have been investigated. The results have been compared with various theoretical models, including the steady state model[11-13], flow model[14], sheath models[15,16] and for collisionless plasmas[17,18].

This paper discusses axial flow and end losses in a collisional plasma with no externally applied magnetic mirrors or initial bias field, where the plasma is best described by the flow model [14], in which rarefaction or area waves start at each end of the plasma and move inwards towards the midplane. The velocity and change in area and line density across such a wave primarily depend upon beta, sensitively for values close to unity.

Previous studies in this regime include an investigation[19] of particle and heat losses in which experimental results were found to be in agreement with the predictions of an axial version of the one-dimensional M.H.D. code[20]. The relative importance of energy loss due to particle or heat flow has been shown[21] to depend upon the ratio of the mean free path to the coil length. At the values of average beta (0·4) obtained positive identification of rarefaction waves was not possible in the two metre coil used. Rarefaction waves[22] have been observed in a theta pinch of large diameter where $\beta > 0{\cdot}8$ and agreed with calculations using the same code. Waves with sharp area discontinuities have been studied[23] with reversed field where the effective beta is almost unity. Flow effects have also been studied[24] in the formation of a bulged region in a plasma column.

In the experiments described here much better spatial resolution in the axial direction and longer time scales than in previous work have been obtained by using a theta pinch coil 8 metres long in which the plasma remains stable for some tens of microseconds[25]. The theoretical studies have been carried out using, for the first time, an M.H.D code which is two-dimensional in radius and axial length. The assumptions in this code are well satisfied by the collisional 100 eV plasma which is used in the experiment.

The time variation of the computed and measured radial density distributions and line densities at four axial positions has been compared. The numerical calculations were started at 2 microseconds, after the initial dynamic phase, and used the measured plasma distributions at this time as the initial conditions. The subsequent behaviour is then calculated for the measured time variation of the external magnetic field. In general, the experimental results including the propagation of rarefaction waves are in agreement with computed predictions.

2. THEORY

2.1 Two-dimensional M.H.D. Code[26]

This code was designed to study the axial flow of heat and particles and it describes the time history of the discharge after the initial implosion phase. A collision-dominated one-fluid plasma with infinite electrical conductivity and isotropic pressure is assumed. The M.H.D. equations are used and hence the set of differential equations for the quantities ρ, $\vec{v}$, p and B are:

$$\frac{\partial}{\partial t}\rho + \nabla.(\rho\,\vec{v}) = 0$$

$$\rho\left(\frac{\partial}{\partial t}\vec{v} + (v.\nabla)\,\vec{v}\right) + \nabla p - \frac{1}{c}\vec{j}\times\vec{B} = 0$$

$$\frac{\partial}{\partial t}p + (\vec{v}.\nabla)p + (\gamma-1)\,p(\nabla.\vec{v}) - (\gamma-1)\,\nabla.(\kappa\,\nabla T) = 0 \qquad \ldots (1)$$

$$\frac{1}{c}\frac{\partial}{\partial t}\vec{B} = -\nabla \times \vec{E}$$

$$\frac{4\pi}{c}\vec{j} = \nabla \times \vec{B}$$

$$\nabla.\vec{B} = 0$$

$$\vec{E} + \frac{\vec{v} \times \vec{B}}{c} = \eta \vec{j} = 0$$

where ρ = mass density, v = flow velocity, p = pressure, B = magnetic induction vector, j = current, $\gamma = \frac{c_p}{c_v}$. The coefficient of heat conductivity is $\kappa = \kappa_i + \kappa_e$ and γ is taken for an atomic gas (i.e. $\gamma = 5/3$). The temperature T is calculated from pressure and mass-density by $T = p/\rho$. Azimuthal symmetry is assumed so that all functions are independent of the angular coordinate θ. It is further assumed that $B_\theta = 0$, $v_\theta = 0$ and that there is no heat flux in the radial direction. The first of these assumptions implies no current flow in the z-direction, while the third is justified because the heat flux along the magnetic field is much greater than that in the perpendicular direction. Radial inertia can be ignored because experimentally after the dynamic phase the radial acceleration is negligible. Therefore the magnetic field is determined by the equilibrium condition

$$-\nabla p + \frac{1}{c}\vec{j} \times \vec{B} = 0 . \qquad \ldots (2)$$

The initial equilibrium conditions for the radial profiles of density and temperature used for the calculations are obtained from experimental data, together with the external magnetic field whose measured time variation is fed into the calculation.

As a boundary condition for the magnetic field at the endplane, periodicity is assumed. For the quantities Y : ρ, $\vec{v}$, p "free boundary" conditions are used, i.e. $\frac{\partial^2}{\partial z^2} Y = 0$.

For the numerical treatment of the system of differential equations the coordinates chosen are (r, z, t). A flux function

$$F(r, z, t) \; := \int_0^r B_z (r', z, t)\, r'\, dr' \qquad \ldots (3)$$

and the corresponding relation between F and the magnetic field $\vec{B}$

$$\vec{B} (r, z, t) = \frac{1}{r} \left\{ - \frac{\partial F}{\partial z} , 0 , \frac{\partial F}{\partial r} \right\} \qquad \ldots (4)$$

suggests the use of the inverted flux function

$$r = R (F, z, t) \qquad (\text{if } B_z \neq 0)$$

as coordinate lines (instead of r = const). This curvilinear coordinate system is non-orthogonal and time-dependent. Its main advantage is that a more accurate computation of effects parallel to the magnetic field lines is possible because there is no numerical diffusion perpendicular to F = const. Infinite electrical conductivity implies no transport of plasma across the coordinate lines f = const particularly at the plasma/vacuum interface, since it is a flux tube. Therefore the only velocity in the radial direction is the velocity of the coordinate lines, which simplifies the set of differential equations.

The numerical solution of the equations in this coordinate system is obtained by solving the equivalent difference approximation. Implicit methods are used for the equations of ρ, v, p. The equation for radial equilibrium is solved with an iterative method.

2.2 Theoretical Results from 2D Code - Comparison with Analytic Model

Firstly the computed velocity of the rarefaction wave is compared, for an experimental diffuse density profile (examples are shown in Section 4), with the analytic results of Wesson's flow model[14]. There

are differences in the assumptions in these two calculations principally that in the flow model radial uniformity and a constant external magnetic field are assumed, and thermal conductivity is neglected. However, by normalising the computed quantities the gross effects of the time-varying external field can be removed and the comparisons are made for individual flux tubes. For $T \sim 100$ eV additional 2D calculations show that thermal conduction can be neglected.

The analytic model predicts that area waves will travel from the ends of the midplane with a velocity[+]

$$V_s = c_s \sqrt{1 - \beta} \qquad \ldots (5)$$

where c_s is the sound speed. The area ratio across this wave is

$$A = [(1 - \beta)/\gamma]^{-\frac{1}{3}} . \qquad \ldots (6)$$

When $\beta \lesssim 0{\cdot}8$–$0{\cdot}9$ the change in line density across the wave is mainly due to the change in the number density, while for higher values the change in line density results from a large change in the plasma area.

The value of V_s on three flux tubes was obtained directly from the 2-dimensional calculations and compared with the phase velocity V_p of the wave on the same flux tubes defined by

$$V_p = \frac{\Delta z}{\Delta t}$$

where Δt is the interval between the times at which the normalised density, $n^* = n/n_o$, (suffix o referring to the start of the computation) and the normalised line density, $N^* = N/N_o$, have fallen by 3% at two axial positions a distance Δz apart ($\Delta z = 50$ cm). In Table 1 the wave velocities are shown for flux tubes at mesh points

+ The simple expressions given are for the case that the effect of the conducting coil can be neglected, which applies for the compression ratios in this work.

1, 13 and 25, for distances z = 100, 150 and 200 cm from the ends. Mesh point 1 corresponds to the axis, point 13 to about 1·25 cm where the density has fallen to approximately 18%, but the temperature (~ 100 eV) remains constant; point 25 refers to radii about 2·5 cm where both the density and temperature have fallen to values less than 5% of those at the plasma axis. No analytic results for the line density wave are given because the appropriate average values of c_s and β are not known. It is seen from Table I that the wave velocity is a minimum on the axis where beta is largest and rises to a maximum at point 13, since β has decreased, although the temperature and sound speed remain constant. At point 25 the velocity has decreased again because the temperature has fallen and the reduction in sound speed outweighs the $\sqrt{1-\beta}$ factor in equation (4).

Table I illustrates that qualitatively according to the 2D code the plasma, on a given flux tube, is lost according to the local values of sound speed and beta, which supports the supposition that the analytic model can be applied on individual flux tubes for a diffuse density distribution. The most reliable quantitative comparison between the two models is expected on the axis and at mesh point 13. In the two cases at z = 150 cm and in the one case at z = 200 cm the agreement is within 10%. However, at axial positions which are closer to the coil ends (z < 150) the agreement is less good and the code shows higher values for the velocity, which is believed to be due to the end effects - for example, insufficient mesh points covering the initial phases of the wave. The agreement shown in Table I could only be obtained when the maximum number of axial mesh points (50) was used. Further studies showed that the results varied considerably when the number of mesh points was reduced, for example, with 25 points

the value of the velocity of the line density wave was larger by a factor of 1·8. According to the analytic model the density should begin to fall sequentially at different axial positions with the arrival of the rarefaction wave. This effect, seen in Fig.1, was only clearcut using 50 mesh points; with significantly fewer points it was smeared out and the line density tended to fall simultaneously at all axial positions. With 50 mesh points the accuracy was better than 15-20%, and using a hyperbolic extrapolation agreement with the analytic model to less than 10% was obtainable.

3. EXPERIMENTAL DETAILS AND PLASMA PROPERTIES

The experiments were carried out on a theta pinch with the coil 771 cm in length and internal diameter 11 cm which encircles a quartz tube of 8·1 cm bore, filled with deuterium gas at an initial pressure of 20 mtorr[27]. The peak magnetic field of 21 kG was reached in 5·5 μsec and e-folded in about 160 μsec.

The radial density distribution (the line density is obtained by integrating the profile) was measured at the midplane and at four other axial positions from an Abel inversion of the light intensity profile obtained from streak photographs using a calibrated image converter camera[27]. The temperature distribution was measured at the midplane using Thomson scattering and the mean value agreed with that obtained from diamagnetic loops assuming $T_e = T_i$. The radial density distribution was of Gaussian form and the radial temperature distribution was uniform over most of the plasma[27]. The plasma in the midplane was found to be uninfluenced by either particle or heat losses for at least 25 μsec; the expected time of arrival of the rarefaction wave was at least 40 μsec.

The plasma density on axis at peak field is $2{\cdot}7 \pm 0{\cdot}3 \times 10^{16} cm^{-3}$ with equal ion and electron temperatures of 120 ± 12 eV. The plasma is collision dominated with $\tau_{ii} \sim 0{\cdot}1 \mu sec$, $\tau_e \sim 2$ μsec; beta on the axis is about 0·7 with an average value[25] of about 0.4: the ion Larmor radius is about 1 mm and the mean plasma radius is about 1 cm.

This plasma is well described by ideal hydromagnetic theory and satisfies the principal assumptions in the 2-dimensional computational model (Section 2.1), namely isotropic pressure and equal ion and electron temperatures. The assumption of infinite electrical conductivity is also justified, because for the observed classical diffusion[28] in the midplane the density distribution does not change (from diffusion) over the times for which end losses were studied.

4. EXPERIMENTAL RESULTS AND DISCUSSION

Fig.2 shows radial image converter streak photographs taken at distances of z = 50 and 100 cm from the ends with a time resolution 0·5 μsec. The change in area due to the rarefaction wave becomes marked by about 10 μsec at z = 50 cm. The lateral motion seen at z = 50 and 100 is an m = 1 instability believed to be associated with the adverse curvature of the magnetic field lines due to the m = 0 rarefaction wave, which propagates faster than the m = 1 wave[25]. This motion was similar to that of the m = 1 instability propagating outwards from a deliberately introduced m = 0 bulge in the midplane of the coil[25]. Its amplitude is less than the plasma diameter and decreases with axial distance from the ends; it does not appear to affect the density profile nor give rise to radial particle losses.

Measured density distributions are compared with those calculated using the 2-dimensional code in Figs.3 and 4 at various axial positions

and different times. The computations were started at 2 μsec, after the implosion (duration ~ 1 μsec) and when radial oscillations have damped out; the initial conditions are the measured radial distributions of temperature and density at that time (on axis 85 eV, $1{\cdot}6 \times 10^{16} cm^{-3}$).

Fig.3 shows that, for z = 50 cm and at five different times after the rarefaction wave has reached this position (which occurs at about 5 μsec) the computed and measured distributions are in reasonable agreement. Each curve shown comes from one discharge, and the errors shown correspond to standard deviations over five similar discharges which were about ± 10%. The time variation of the profile largely depends on that of the external magnetic field; the effect of end losses is superimposed on this variation. Fig.4 shows the computed and measured distributions at 13·4 μsec for three axial positions. Agreement is within the experimental error at z = 50 and 100 cm, but at z = 200 cm it is less good.

Fig.5 shows for four axial positions that the time variation of the computed and measured line density, normalised to the initial value, agrees to within the experimental error. The principal characteristics of rarefaction waves expected from Wesson's [14] analytic theory can be seen; the line density remains constant at a given position until the rarefaction wave reaches this point, when it begins to fall. A sequential decrease of the line density with increasing z is seen for z = 50, 100 and 150 cm. There is some evidence from Fig.5 that the theoretical curves fall sooner than expected, corresponding to a faster area wave velocity than the analytic theory predicts, especially at smaller values of z, as was mentioned in Section 2.2.

The experimental data shows a similar trend but, taking into account the experimental error and the uncertainty about the time at which axial plasma flow begins, it was not possible to resolve whether or not this was a genuine effect.

Fig.6 shows, at a position 50 cm from the end, the experimental and computed time variation of the line density and the number density on the axis; theory is also shown for n_e at mesh point 13, a flux tube at a radius of about 1·25 cm. Each computed value of the number density is normalised with respect to the value at the same mesh point and the same time in the unperturbed plasma. The same (computed) normalisation factors are used for the experimental data, since larger normalisation errors would have been introduced by normalising with respect to other experimental data because measurements were only made at one value of z per discharge. It is seen that the computed curves for the line density and the density at mesh point 13 lie close together, which implies that the values of density and beta on that flux tube are characteristic of the plasma as a whole from the point of view of end losses. The theoretical curve for the density on the axis lies some 20% higher than that at mesh point 13 which confirms the conclusion from Table I that particles are lost according to the local values of beta and the sound speed, the effect of beta dominating in the present experiment. The experimental data for the density on the axis shows a spread extending outside the experimental error possibly because of the normalising process. However, qualitatively the data in Fig.6 shows that particles on the axis are lost more slowly than in the plasma as a whole. This is known as the 'onion skin' effect and has not previously been observed.

5. CONCLUSIONS

Observations on axial flow of plasma and end losses in a collision dominated plasma at 100 eV in a theta pinch are in general agreement with the predictions of a 2-dimensional M.H.D. code, whose essential assumptions are well satisfied experimentally.

The propagation velocities of the rarefaction wave for the density on different flux tubes computed from the 2D code and obtained from Wesson's[14] one-dimensional analytic model agree. The agreement is within 10-15% for distances more than 100 cm from the ends of the coil using the maximum number of 50 mesh points in the axial direction.

The measured time variation of the electron density distribution at different axial positions along the coil agrees remarkably well with the computed distributions, often to better than 10% which is less than the combined experimental and numerical error. Rarefaction waves were found experimentally and the line density fell sequentially at successive axial positions as the waves travelled from the ends to the midplane, in satisfactory agreement with the 2D code. The measured time variation of the number density on the axis was in approximate agreement with numerical predictions which showed that particle flow on a given flux tube is determined by the local values of beta and sound speed, a result expected but not previously demonstrated. Higher beta plasma near the axis is lost more slowly than the plasma as a whole.

ACKNOWLEDGEMENTS

The authors wish to thank J.A. Wesson and A.A. Newton for useful discussions and Mrs J.E. Crow for assistance with the computing.

REFERENCES

1. H.A.B. Bodin, T.S. Green, A.A. Newton, G.B.F. Niblett, J.A.Reynolds, in Plasma Physics and Controlled Nuclear Fusion Research, (International Atomic Energy Agency, Vienna, 1966), Vol.1, p.193.
2. W.B. Jones, L.M. Goldman, R.W. Kilb and R.L. Bingham, Phys. Fluids 13, 800 (1970).
3. A. Heiss, H. Herold, E. Unsöld, Bull. Am. Phys. Soc. 12 1158 (1967).
4. E.M. Little, W.E. Quinn, G.A. Sawyer, Phys. Fluids 8, 1168 (1965).
5. K.S. Thomas, Phys. Fluids 11, 1125 (1968).
6. A.C. Kolb, W.H. Lupton, R.C. Elton, E.A. McLean, M. Swartz, M.P. Young, H.R. Griem, E. Hintz, in Plasma Physics and Controlled Nuclear Fusion Research (International Atomic Energy Agency, Vienna, 1966), Vol.1, p.261.
7. E.A. McLean, A.D. Anderson, H.R. Griem, Proceedings APS Conference on Pulsed High Density Plasmas, LA 3770/A5 (1967).
8. H.A.B. Bodin, C. Bunting, Culham Report CLM-R 70 (1967).
9. A.C. Kolb, M.P. Young, E.A. McLean, Proceedings APS Conference on Pulsed High Density Plasmas, LA 3770/G 5 (1967).
10. J.W. Mather, Nuclear Fusion 1, 233 (1961).
11. N.J. Phillips, J.K. Wright, Plasma Physics (J. Nuclear Energy Part C) 1, 240 (1960).
12. K.V. Roberts, Plasma Physics (J. Nuclear Energy Part C) 1, 243 (1960).
13. J.B. Taylor, J.A. Wesson, Nuclear Fusion 5, 159 (1965).
14. J.A. Wesson, in Plasma Physics and Controlled Nuclear Fusion Research (International Atomic Energy Agency, Vienna, 1966), Vol.1, p.223.

15. J.B. Taylor, Culham Report CLM-R 58 (1966).

16. I.J. Spalding, In Advances in Plasma Physics, vol.4, edited by A. Simon and W.B. Thompson. Published by John Wiley & Sons, Inc. 1971, pp.79-123.

17. W. Grossman, Phys. Fluids 9, 2478 (1966).

18. R.L. Morse, Phys Fluids 9, 2536 (1966).

19. T.S. Green, D.L. Fisher, A.H. Gabriel, F.J. Morgan, A.A. Newton, Phys. Fluids, 10 1663 (1967).

20. G. Hain, K. Hain, K.V. Roberts, S. Roberts, W. Koppendorfer, Zeits. fur Naturforschung, 15a, 1039 (1960).

21. R.J. Bickerton, Culham Memorandum, CLM-M-35 (1964).

22. A.A. Newton, Nuclear Fusion 8, 93 (1968).

23. H.A.B. Bodin, T.S. Green, G.B.F. Niblett, N.J. Peacock, J.M.P. Quinn, J.A. Reynolds, J.B. Taylor, Nuclear Fusion Supp.2, 511 (1962).

24. J. McCartan, G.H. Wolf, H.A.B. Bodin, Plasma Physics 12, 885 (1970).

25. H.A.B. Bodin, A.A. Newton, G.H. Wolf, J.A. Wesson, Phys. Fluids 13, 2735 (1970).

26. W.H. Schneider, F. Hertweck, Garching Report IPP6/90 (1970).

27. A.D. Beach, H.A.B. Bodin, C.A. Bunting, D.J. Dancy, G.C.H. Heywood, M.R. Kenward, J. McCartan, A.A. Newton, I.K. Pasco, R. Peacock, J.L. Watson, Nuclear Fusion 9, 215 (1969).

28. H.A.B. Bodin, A.A. Newton, Phys. Fluids 12, 10 (1969).

TABLE I

	V (n^*(m=1)) cm/sec	V (n^*(m=13)) cm/sec	V (n^*(m=25)) cm/sec	V (N^*) cm/sec	z
2D	8.40	14.18	11.23	13.50	100
Analytic (Wesson)	7.52	10.90	7.58	-	
2D	7.66	12.06	9.78	11.48	150
Analytic (Wesson)	7.65	10.92	8.13	-	
2D	*	11.81	10.31	11.12	200
Analytic (Wesson)	*	11.30	7.93	-	

* Computation did not extend far enough in time to cover this case

Table Caption

Comparison between wave propagation velocities V obtained using the analytical expression[14] and numerically from the two-dimensional code, at three axial distances z , measured from the coil end. The normalised line density, N^*, and the normalised number density, n^*, on three flux tubes (mesh points m = 1, 13 and 25, corresponding to the axis, radii about 1·3 cm and 2·4 cm) are shown.

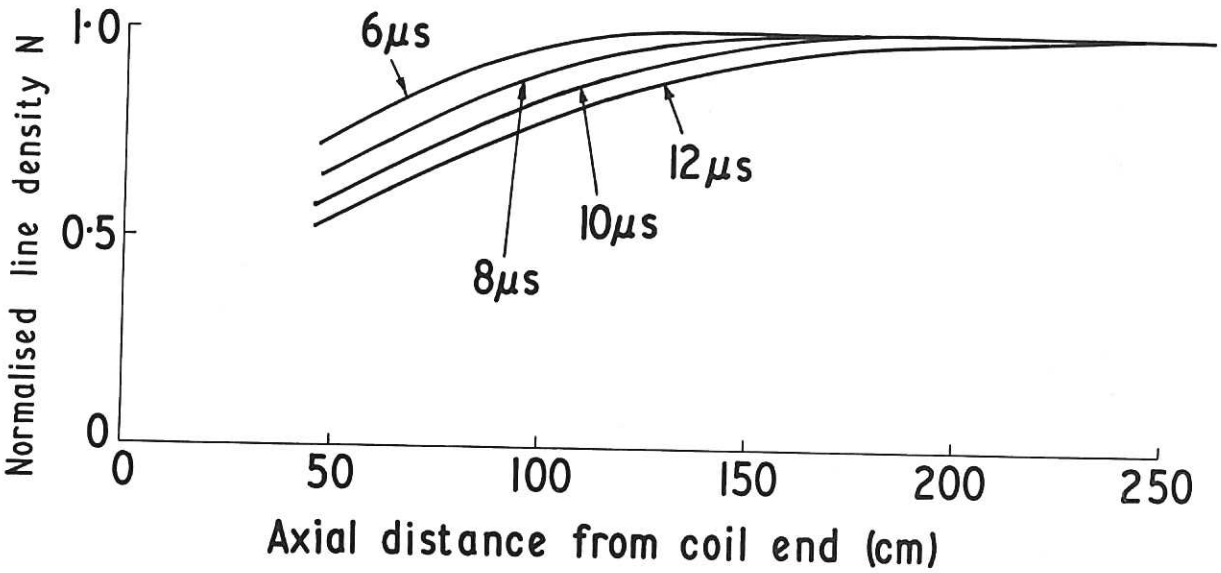

Fig. 1 Computed axial variation of line density at different distances from the coil end showing the propagation of a rarefaction wave from the end towards the midplane.

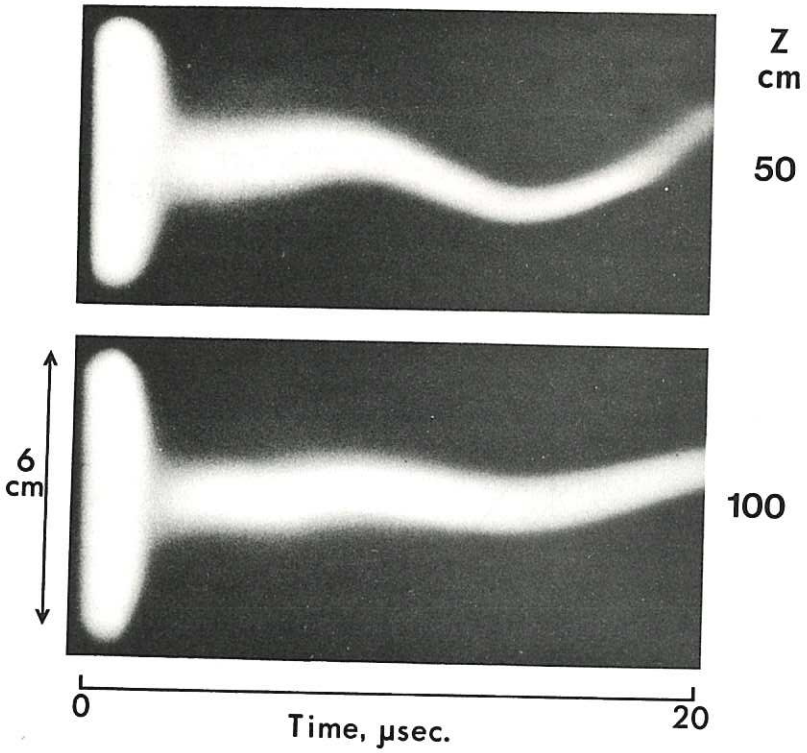

Fig. 2 Streak photographs taken at two axial positions z = 50 and 100 cm from the end of the coil.

CLM-P283

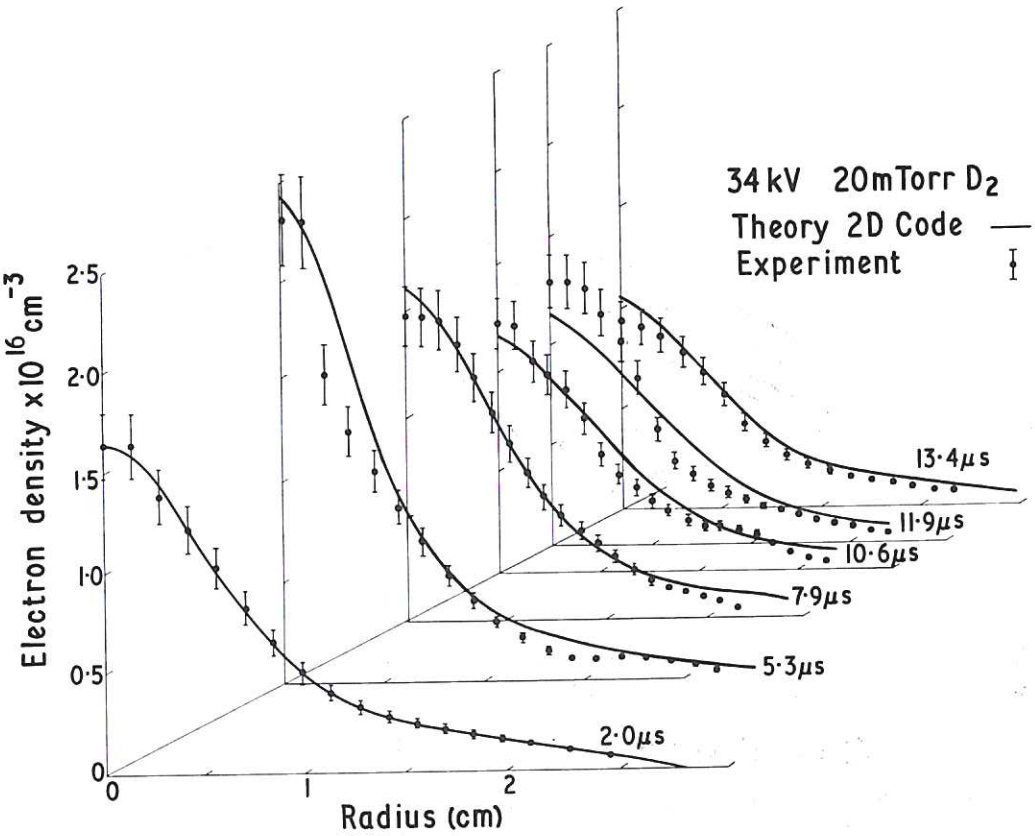

Fig. 3 Time evolution of density distribution at z = 50 cm from the end of the coil. Experiment and theory, 2D code.

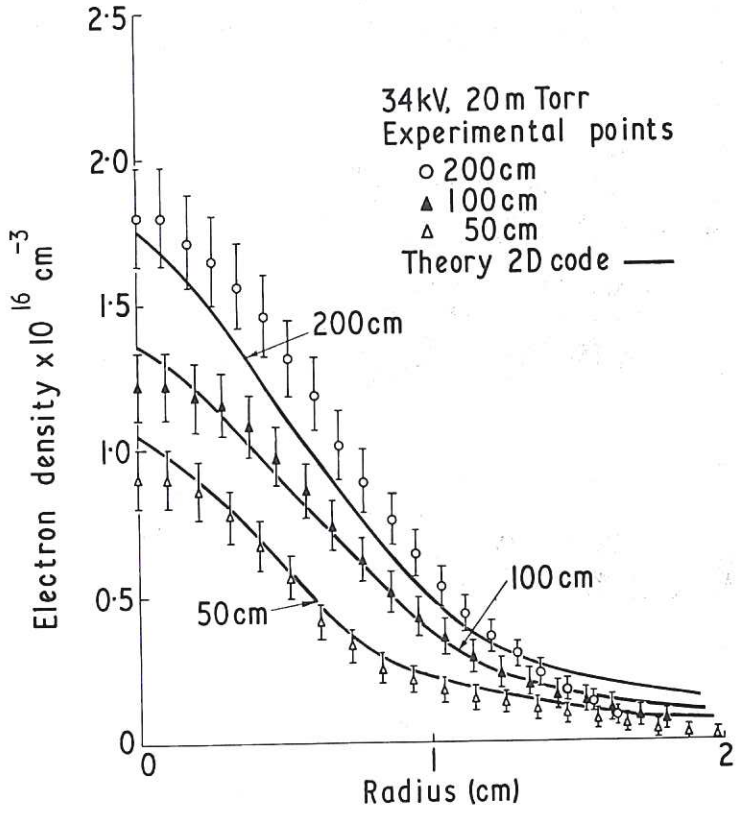

Fig. 4 Radial density distributions at 13 microseconds for 3 axial positions from the end of the coil. Experiment and theory, 2D code.

CLM-P283

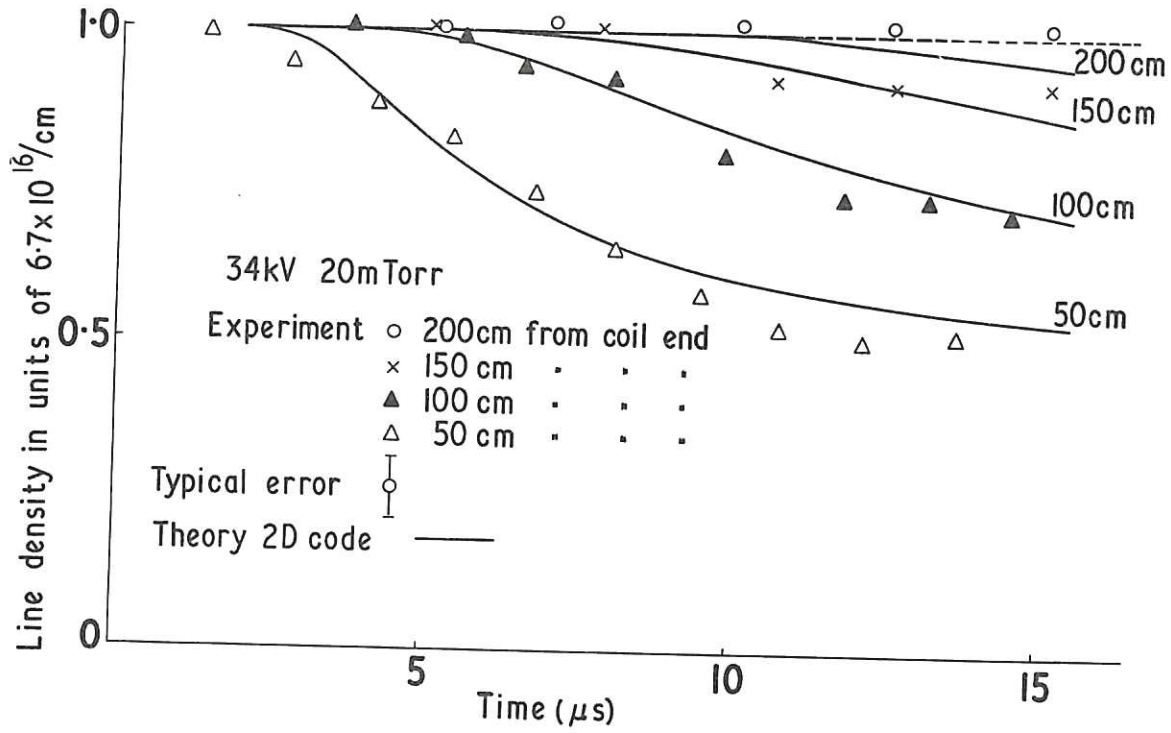

Fig. 5 Time variation of the line density at 4 axial positions; experiment and theory, 2D code.

CLM-P283

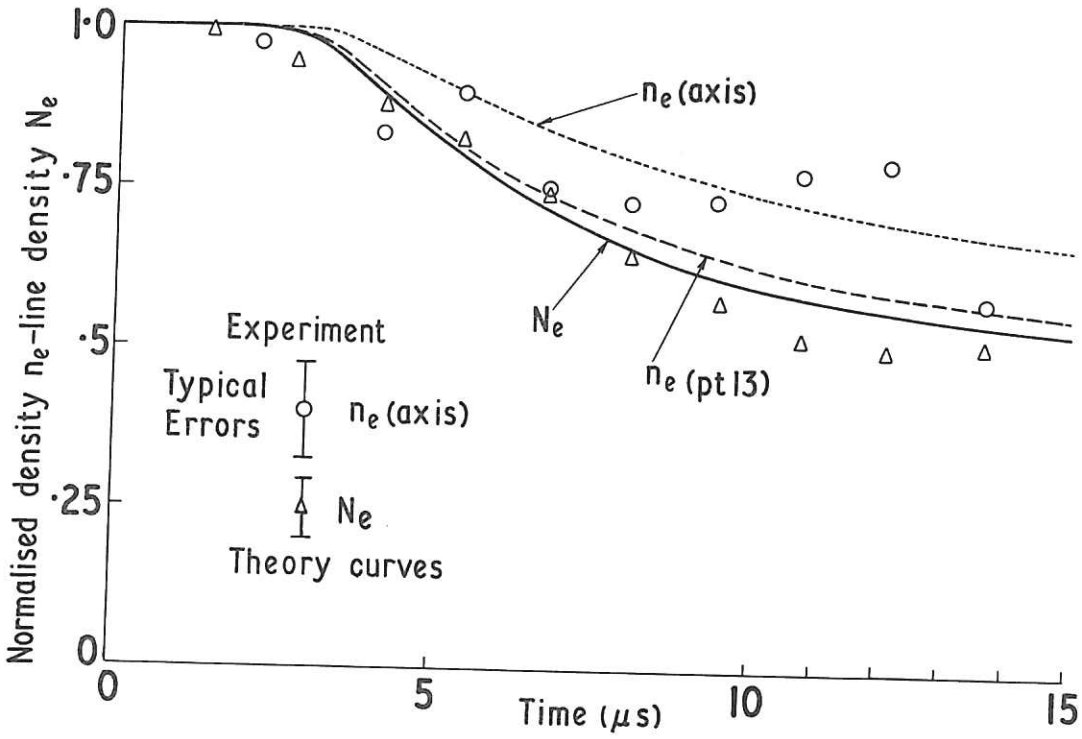

Fig. 6 Computed time variation of the line density and the number density on axis and at mesh point 13; experimental data for the density on axis and the line density is also shown. (z = 50 cm from the end of the coil.)

CLM-P283